JASA ARTICLE

Underwater sound levels of transiting crew transfer vessels

Fritjof Basan,[1,a] Christ A. F. de Jong,[2] Christian Krüger,[1] and Jens-Georg Fischer[1]
[1]Federal Maritime and Hydrographic Agency (BSH), Hamburg, Germany
[2]Netherlands Organization for Applied Scientific Research (TNO), The Hague, The Netherlands

ABSTRACT:
Underwater sound recordings from Helgoland, Germany, were analyzed to detect passages of crew transfer vessels (CTVs). From these opportunistic observations, the source levels of 13 individual vessels were derived using the smoothed semi-coherent image method, including frequency-dependent absorption. Statistical analysis, using both generalized additive models and random forest models, showed that vessel-specific differences are the primary source of variability in source levels. While speed, length, and propulsion type all influence source levels, their effects vary across vessels and frequency bands, with no single factor dominating overall. The results indicate that, despite their relatively small size, CTVs have radiated noise levels similar to larger cargo vessels. The low variability in source levels across vessels suggests that a single source level spectrum for transiting CTVs could be a viable input for future noise modelling efforts.
 https://doi.org/10.1121/10.0043324
(Received 25 September 2025; revised 21 January 2026; accepted 16 March 2026; published online 17 April 2026)
[Editor: James F. Lynch] Pages: 3406–3415

I. INTRODUCTION

Anthropogenic underwater noise has been recognized as a key environmental stressor for marine life, affecting the communication, foraging, and navigation of marine organisms (Duarte *et al.*, 2021; Erbe *et al.*, 2018; Hawkins and Popper, 2017). In the North Sea, the rapid expansion of offshore wind farms has led to increased vessel traffic for both construction and maintenance activities. Although the noise impacts of construction activities, especially pile driving, are well documented as a major disturbance to marine mammals (Brandt *et al.*, 2011) and are subject to strict regulatory measures (Juretzek *et al.*, 2021), continuous noise emissions from service vessels, including crew transfer vessels (CTVs), remain less well understood. Depending on distance to shore and operational requirements, wind farm maintenance is carried out by service operation vessels (SOVs) or CTVs (McMorland *et al.*, 2022). CTVs, which are typically high-speed catamarans with azimuth pod (AP) or propeller propulsion, play a central role in servicing offshore wind farms in the German Exclusive Economic Zone, particularly around Helgoland. Previous studies suggest that small, high-speed vessels can generate significant noise emissions, particularly in higher-frequency bands relevant to marine mammal communication (Hermannsen *et al.*, 2025). However, comprehensive measurements of CTV source levels (SLs) and their dependences on vessel-specific parameters are scarce. To address this knowledge gap, we analyzed passive acoustic recordings from two autonomous recorders deployed north of Helgoland over a 4-month period. Using the smoothed semi-coherent image (SSCI) method (Yubero *et al.*, 2025), extended with a standard frequency-dependent absorption term to ensure accurate high-frequency propagation, we calculated SLs and deep water radiated noise levels (RNLs) for 13 individual CTVs. To provide a consistent reference scale for contextualizing the measured RNLs, we compare the resulting spectra to the RNL curve of a typical large commercial vessel (a 200 m bulker travelling at 14 kn), computed following MacGillivray and de Jong (2021).

Based on the JOMOPANS-ECHO (J-E) model (MacGillivray and de Jong, 2021), vessel SLs are expected to primarily depend on vessel class, speed, and length. Prediction of the SL of a CTV is uncertain, because the database that was used for the development of the J-E model does not include CTVs or similar vessels. This study provides empirical data to improve underwater noise models for offshore wind farm service vessels. As part of the EU Interreg North Sea Region DEMASK Project (2025), our objective is to refine noise prediction methodologies by facilitating the implementation of CTV service traffic in existing models. By improving the understanding of CTV noise emissions, this research contributes to regulatory frameworks and marine spatial planning in the North Sea.

II. METHODS

After describing the measurement location and data collection process (Secs. II A and II B), we detail the identification of CTV passages in the acoustic data in Sec. II C. The subsequent sections explain the calculation of SLs and RNLs using the SSCI method, including frequency-dependent absorption correction (Sec. II D), followed by

[a]Email: fritjof.basan@bsh.de

https://doi.org/10.1121/10.0043324

statistical analysis using generalized additive models (GAMs) and random forest (RF) models (Sec. II E).

A. Measurement setup

Selecting an appropriate measurement location was crucial to maximize the number of recorded CTV passages. To identify a suitable site, automatic identification system (AIS) data from the JOMOPANS Project (2020) were analyzed, focusing on tracks of vessels classified as "high-speed crafts."

Helgoland serves as a key departure point for CTVs, servicing four offshore wind farms to its north: Amrumbank West, Kaskasi II, Nordsee Ost, and Meerwind Süd/Ost. Given its strategic position and high vessel traffic, a measurement site was chosen within the northern approach fairway to Helgoland.

To minimize the risk of equipment loss due to fishing activity, additional AIS data from the JOMOPANS Project were reviewed to avoid high-density fishing areas. The selected measurement location is shown in Fig. 1. Two hydrophones were deployed at this site, positioned 60 m apart to ensure data redundancy. Recordings were collected continuously from June 24 to October 08, 2024. The black lines in Fig. 1 indicate the AIS-tracked CTV passages recorded during this period.

The recorders were installed in custom-made cages that were held vertically in the water column with floating buoys. Both recorders were measuring for 55 min every hour, ensuring sufficient time for the recorder to properly save the audio files in WAV format. The sensitivity of the recorders was tested prior to deployment using a custom-made acoustic calibrator at 125 Hz (IEC, 2019). The sample rate was set to 96 kHz, enabling an analysis of decidecade bands up to 40 kHz. Table I provides an overview of the location of the measurement, the equipment used, and the settings chosen.

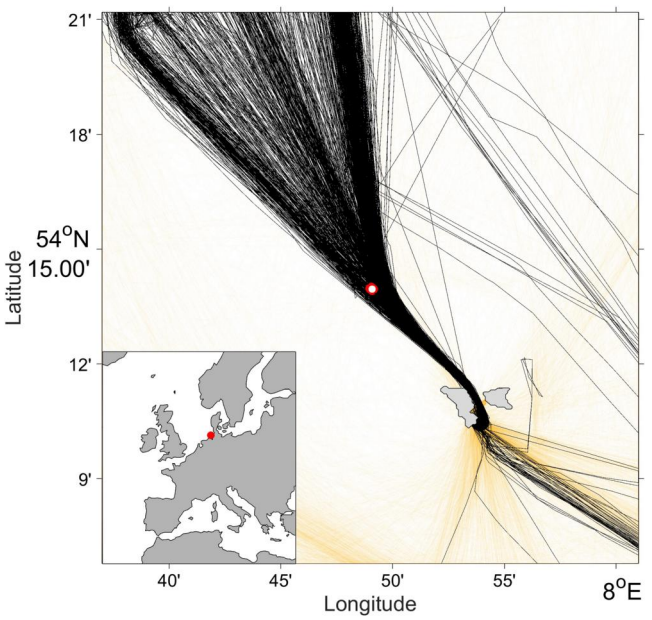

FIG. 1. Tracks of crew transfer vessels around Helgoland (black) and other marine traffic (orange) between June and October 2024.

TABLE I. Overview of measurement location and used equipment.

Parameter	Recorder 1	Recorder 2
Latitude	54.23°N	54.23°N
Longitude	7.82°E	7.82°E
Water depth	24.8 m	24.5 m
Recorder type	SoundTrap ST600	SoundTrap ST600
Sampling rate	96 kHz	96 kHz
Duty cycle	55 min/1 h	55 min/1 h
Sensitivity	−177.7 dB re 1 V/μPa	−177.9 dB re 1 V/μPa

B. Data collection and preprocessing

The raw data files were quality controlled following the recommended practice from Ward *et al.* (2021). Then all recordings were processed to compute 1-s sound pressure levels (SPLs) for all decidecade frequency bands between 10 Hz and 40 kHz using the tool BSOUNDH, developed by Fraunhofer IDMT (Oldenburg, Germany) during the BSH SOUND Mapping Project (2021). The tool uses an integrated filter bank and was tested to conform with the common standards (IEC, 2014, 2016).

C. Identification of CTV passages

AIS data, sourced from the European Maritime Safety Agency (EMSA), were analyzed to identify vessel passages where the distance of the closest point of approach (DCPA) to the hydrophone was less than 1 km (mean DCPA 429 m, standard deviation 229 m). Only passages without other vessels within 2 × DCPA were considered, resulting in the identification of 3243 passages, of which 2526 were CTV passages. To correlate these passages with the acoustic data, peaks in the broadband SPL time series were identified within ±2 min of the time of the closest point of approach (TCPA) for all passages. Only peaks with a minimum prominence of 6 dB above their local acoustic background were considered, where prominence is defined as the level difference between a peak and the lowest surrounding local minimum. All 810 preselected peaks were then manually validated using a custom MATLAB interface (see Fig. 2). The closest point of approach (CPA) for each passage was determined by examining the narrowband spectrogram up to 1000 Hz. Specifically, the minimum of the characteristic U-shaped interference pattern—known as the Lloyd's mirror effect, which results from the interference between direct and surface-reflected sound paths—was manually identified (Urick, 1983). However, manual selection of these minima was complicated by uncertainties that may arise from frequency-dependent effects, the directional characteristics of the sound source, or its relative position and motion.

The shift between manually validated TCPAs and TCPAs from the AIS data reveals a constantly increasing time drift between the recorders and the AIS data. Both recorders exhibit a similar clock drift (Fig. 3). A linear

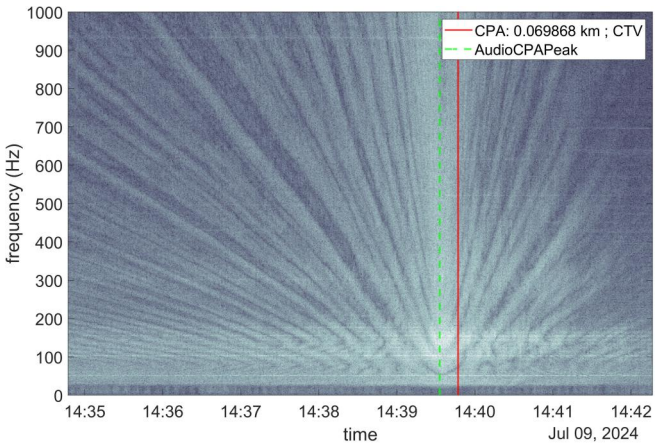

FIG. 2. Example of the user interface that was used to manually select and verify the TCPAs in the acoustic data. The red line indicates TCPA from AIS data, and the dotted green line indicates TCPAs from the interference pattern analysis.

regression for the clock drift was calculated, and all passages with ΔTCPAs greater than 1 standard deviation were discarded from further analysis. These passages were excluded due to potential uncertainties in their data, such as inaccuracies in the AIS timestamps. Clock drift is a well-known phenomenon in autonomous recorders and has been reported in previous studies using SoundTrap devices (Ocean Instruments NZ, Auckland, New Zealand). For example, Malinka *et al.* (2020) observed a drift of approximately 2 s/day for a SoundTrap ST300 recorder deployed in deep water, while Macaulay *et al.* (2020) reported a drift of 72 ms/h (equivalent to ca. 1.72 s/day) for a SoundTrap ST500 recorder. In contrast, the recorders used in this study exhibit a significantly lower drift, with values of 0.5 s/day (0.021 s/h) for recorder 1 and 0.47 s/day (0.0197 s/h) for recorder 2. This suggests that either newer device models have improved internal clock stability, or different deployment conditions (e.g., shallower depth or higher temperatures) contributed to the reduced drift. The remaining 750 CTV passages were used for subsequent analysis.

TABLE II. Overview of identified CTV passages.

Parameter	Value
No. of identified CTVs	13
CTV length range	22–32 m
CTV draught range	1.1–2.3 m
Assumed source depth range	0.8–1.6 m
No. of passages per CTV	4–94
Speed range during passages (kn)	10–25 kn

All identified CTVs were measured during transit. Table II summarizes the number of vessels, their length range, the number of passages per vessel, and the observed speed range during the passages.

D. Acoustical analysis

There are well-established standards on how to measure radiated noise of cooperating vessels in deep water and for deriving SLs (ISO, 2016, 2019). The newly published ISO 17208-3 builds upon these standards and describes procedures for ship noise measurements in shallow water, including the use of the SSCI approach for propagation loss

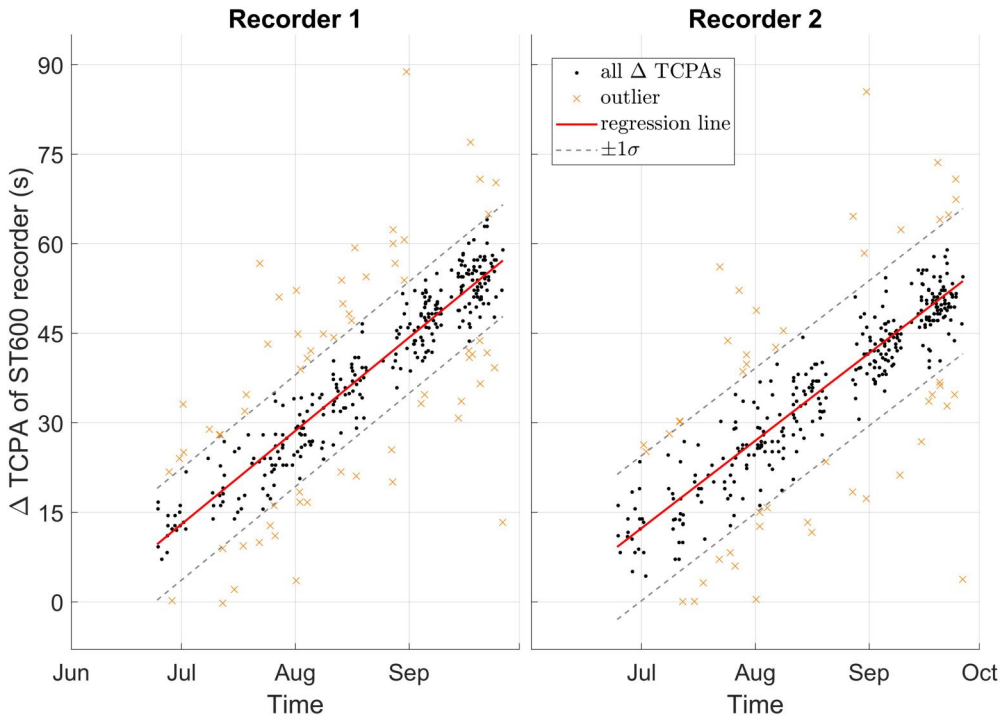

FIG. 3. Difference of TCPAs (ΔTCPA) between the TCPA in AIS data and manually identified TCPAs in audio data; the red line in each panel indicates the trend line, i.e., time drift of each recorder. Only TCPAs within 1 standard deviation of the fitted trend were included in the analysis.

https://doi.org/10.1121/10.0043324

estimation (ISO, 2025). However, no international standard currently exists for opportunistic underwater radiated noise measurements from transiting vessels. In this study, ISO 17208-3 was used as a methodological framework for opportunistic shallow water ship-noise measurements.

All validated CTV passages were processed as described in the following. A data window period (DWP) was defined around each manually validated TCPA. The DWP corresponds to the time during which the vessel remained within a $\pm 30^\circ$ sector centered around the CPA. The length of this data window (DWL) is defined as

$$l_{\mathrm{DW}} = 2\tan(30^\circ) d_{\mathrm{CPA}}. \tag{1}$$

Consequently, the DWP is given by

$$t_{\mathrm{DW}} = \frac{l_{\mathrm{DW}}}{v}, \tag{2}$$

where v is the speed of the passing vessel. All 103 passages with DWPs shorter than 10 s were excluded from further analysis. Mean-square SPLs were calculated for all passages over their respective DWPs. The background noise level during each passage was defined as the 5th percentile of the SPLs over a period of 60 min around the TCPA. The corresponding background noise levels per frequency band were subtracted from the measured signal within the DWP. Only passages where the signal exceeded the background noise level by at least 3 dB across all frequency bands were considered for further analysis, resulting in a total of 529 passages included in the final dataset. In practice, more than 95% of passages exceeded the background by ≥ 6 dB in all bands, indicating that background-noise bias is negligible.

To calculate SLs from these background-noise-corrected SPLs, L_p, the propagation loss N_{PL} needs to be added,

$$L_{\mathrm{S}}(f_c) = L_p(f_c, d_{\mathrm{CPA}}) + N_{\mathrm{PL}}(f_c, d_{\mathrm{CPA}}), \tag{3}$$

where f_c is the center frequency of the respective decidecade frequency band. According to the ISO 17208-3 standard, the recommended method to determine N_{PL} in shallow water is the SSCI method (ISO, 2025). SSCI combines coherent contributions from the direct path and the first reflections from the sea surface and seafloor with an incoherent sum of contributions from multiple reflected paths.

However, the SSCI formulation neglects frequency-dependent absorption, $\alpha(f)$, and is derived under the assumption that absorption losses over DCPA are negligible compared to geometric spreading (Yubero *et al.*, 2025). Accordingly, ISO 17208-3 and Yubero *et al.* (2025) recommend applying SSCI only within specific applicability limits, namely, for frequencies up to 20 kHz and DCPAs not exceeding 5 × the local water depth.

Because several passages in our dataset exceed the recommended range limits (DCPA >5 × water depth) and frequencies up to 40 kHz were analyzed, absorption cannot be neglected. Following the recommendation of Yubero *et al.* (2025), the SSCI was extended by adding an absorption term,

$$N_{\mathrm{PL}}(f_c, d_{\mathrm{CPA}}) = N_{\mathrm{SSCI}}(f_c, d_{\mathrm{CPA}}) + \alpha(f_c)\, d_{\mathrm{CPA}}, \tag{4}$$

where N_{SSCI} is the SSCI propagation loss estimate and $\alpha(f_c)$ is the absorption coefficient in decibels per meter. $\alpha(f_c)$ was computed using the Thorp parameterization for seawater absorption (Urick, 1983),

$$\alpha(f) = \frac{0.10\frac{f^2}{1+f^2} + 40\frac{f^2}{4100+f^2} + 2.75\times 10^{-4} f^2 + 0.003}{914}, \tag{5}$$

where f is the frequency in kHz. The influence of this absorption correction on SSCI is illustrated in Figs. S2 and S3 in the supplementary material, which quantify the SSCI propagation-loss error relative to the image source model (Urick, 1983) as a function of frequency and range. The figures show that absorption has little influence below approximately 10 kHz, but neglecting it at higher frequencies leads to a systematic underestimation of propagation loss. Using the SSCI-plus-absorption formulation, we obtained SLs for each CTV passage.

Some applications (e.g., quiet ship certification) refer to deep water RNLs rather than SLs. RNL is a standardized, depth-independent noise metric that corrects for source-depth-dependent interference effects and thereby enables consistent comparison across vessels and with literature values. The SSCI-derived SLs were converted to RNLs using the ISO 17208-2 formulation (ISO, 2019)

$$L_{\mathrm{RN}} = L_{\mathrm{S}} + 10\log_{10}\left(\frac{14(kd)^2 + 2(kd)^4}{14 + 2(kd)^2 + (kd)^4}\right) \mathrm{dB}, \tag{6}$$

where $k = 2\pi f_c / c_w$ is the acoustic wavenumber, c_w is the sound speed in water, and d is the source depth in meters. c_w was measured by a nearby BSH measurement frame and extracted for each passage. The source depth was set at 0.7 × the draught of each CTV, which was given in the AIS data and verified from detailed specification sheets per vessel (see Table II).

To contextualize the CTV measurements, we compare the resulting RNL spectra to those of a representative commercial vessel operating in the North Sea—a 200 m bulk carrier travelling at 14 kn. The bulker reference SL spectrum was derived from the empirical J-E SL parameterization (MacGillivray and de Jong, 2021).

E. Statistical analysis

For each passage, AIS provides metadata such as speed over ground (SOG) and vessel length. The J-E model (MacGillivray and de Jong, 2021) predicts SLs as a function of speed and length using the relationship

$$L_{S_f,J-E}(f, v, l) = L_{S_f,0}(f) + 60\log_{10}(v/v_C)\ \mathrm{dB} + 20\log_{10}(l/l_0)\ \mathrm{dB}, \tag{7}$$

where $L_{S_f,0}(f)$ is a baseline spectrum for each vessel class, v is the vessel speed, and v_C is the reference speed for that

class, l is the vessel length, and $l_0 = 300$ ft (91.4 m) is the reference length.

Although the CTVs transited within a constrained range of speeds—their typical transiting speed—and had similar dimensions (Table II; see Fig. 9 below), we tested whether the functional speed and length relationships proposed by the J-E model hold for this vessel class. To assess this, we applied the J-E speed and length scaling to the measured RNLs and subtracted the scaled RNLs from the unscaled RNLs. This difference analysis serves as a sensitivity test of the J-E scaling: If these parameters explained a substantial fraction of the observed variability, applying the scaling would lead to systematic and frequency-dependent changes in the RNL distributions.

Further analysis was conducted using GAM and RF regressions to investigate how speed, vessel length, propulsion type, and DCPA influence CTV SLs. The propulsion type of each CTV was derived from publicly available specification sheets. Both methods allow for analysis of the contribution of individual factors to the observed variability in RNLs (Breiman, 2001; Wood, 2017), with separate models created for each frequency band and for different combinations of explanatory variables to enable a systematic comparison of model performance using adjusted R^2 to account for differences in the number of predictors between models.

III. RESULTS

A. Measured CTV RNL spectra

Figure 4 shows the spectral probability density (SPD) of the measured RNL spectra for all CTV passages (Merchant *et al.*, 2013).

The bulker reference spectrum is included for context. The measured CTV RNLs exceed the bulker RNL over large parts of the spectrum, particularly between 100 and 500 Hz and above 1 kHz. Levels below 25 Hz are affected by flow noise contamination at the hydrophone (not removed by the applied background noise correction), and propagation of these low frequencies is limited in the shallow water environment. The pronounced peak in the 20 kHz band is consistent with the emission characteristics of ultrasonic antifouling devices that may be installed on several CTVs, although this needs to be verified and requires further investigation.

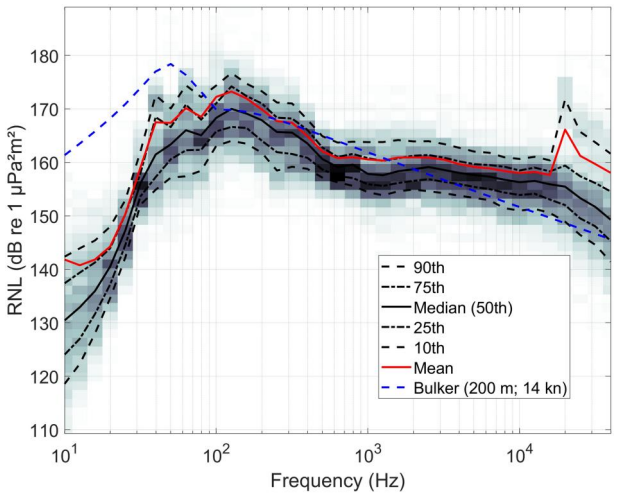

FIG. 4. Spectral probability density (SPD) of RNLs of all CTV passages, compared to a bulker reference RNL spectrum (200 m, 14 kn) used as a spectral benchmark.

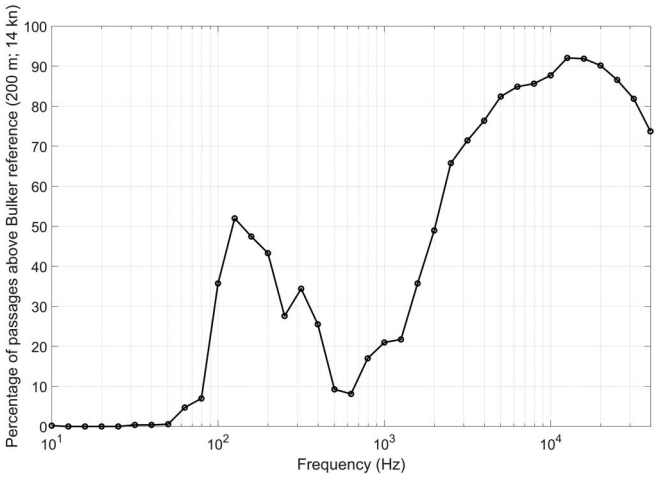

FIG. 5. Percentage of CTV passages for which the measured RNLs exceed the bulker reference spectrum in each frequency band.

Figure 5 illustrates the percentage of analyzed CTV passages for which the measured RNLs exceed the bulker reference spectrum in each frequency band, confirming that exceedances predominantly occur around 125 Hz and 15 kHz.

In general, the measured RNL spectra (Fig. 4) exhibit a relatively low variability, but there are substantial differences between individual vessels. The SPD plots for the 13 individual vessels (see Fig. S1 in the supplementary material) demonstrate that the measured RNLs are broadly comparable in magnitude to the bulker reference spectrum, with all vessels exceeding it in specific frequency bands. The bulker spectrum is used here as a general reference for comparison.

B. Parameter dependence

To evaluate whether the speed and length scaling proposed by the J-E model (MacGillivray and de Jong, 2021) captures a substantial fraction of the observed RNL variability for transiting CTVs, we compared measured RNLs before and after applying the J-E scaling. Figure 6 shows the mean and median differences between scaled and unscaled RNL spectra.

The generally small and weakly frequency-dependent differences indicate that the J-E speed and length scaling removes only a minor portion of the observed variability. This suggests that, within the limited speed and length range of the CTV dataset, RNLs are only weakly controlled by vessel speed and length alone.

Spearman correlation coefficients were calculated to further investigate the relationship between RNLs and

https://doi.org/10.1121/10.0043324

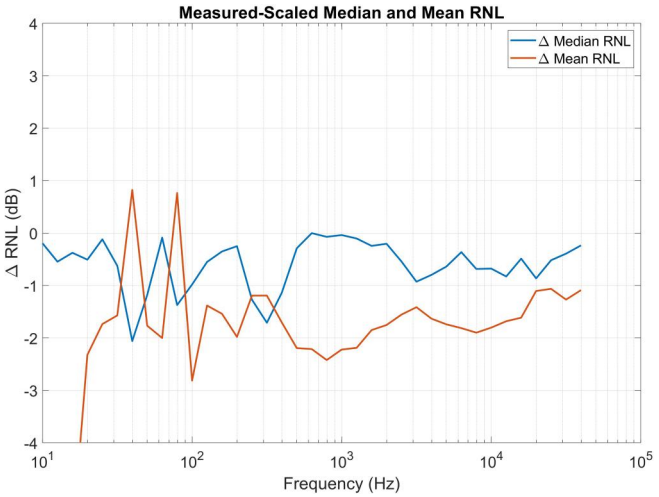

FIG. 6. Differences between J-E scaled and unscaled RNL spectra (mean and median), illustrating the limited effect of J-E speed and length scaling on the observed RNL variability.

vessel speed, length, and DCPA (see Fig. 7). The resulting relationships between RNL, speed, and length are frequency dependent. While speed primarily influences sound levels at 40 and 80 Hz, there is a noticeable trend suggesting that levels above 1 kHz tend to increase with vessel length. However, the maximum correlation of approximately 0.5 is relatively weak, indicating that these bivariate relationships between RNL and individual predictors explain only a limited fraction of the observed variability when considered in isolation.

It is also important to note that ship-specific correlations (gray lines in Fig. 7) differ significantly from the overall correlation for speed. Additionally, the observed trend with vessel length is based on only 13 vessels with a limited range of lengths and is therefore not conclusive. Given the relatively narrow speed distributions in our dataset (10–25 kn) (Table II; see Fig. 9, right panel, below), statistical power to isolate a generic speed effect is inherently limited. The negative correlation between RNL and distance, increasing with frequency, indicates that a residual distance dependence remains in the data. Since a negative correlation means that RNLs decrease with increasing distance, this pattern implies that, particularly at higher frequencies, more distant vessels are associated with systematically lower RNLs.

While the bivariate analyses provide useful first-order insights, they do not capture potential interactions between vessel properties and operational parameters. To address this, we applied GAM and RF regressions per frequency band to assess the relative importance of each parameter. GAMs and RFs were computed across eight different combinations of the following predictors: speed, length, distance, propulsion type, and individual vessel [Maritime Mobile Service Identity (MMSI)]. Three different propulsion types were found for the investigated CTVs: controllable pitch propellers (CPPs), fixed pitch propellers (FPPs), and APs. Model performance was evaluated using the adjusted coefficient of determination (adjusted R^2), which accounts for differences in model complexity and allows a fair comparison between models with different numbers of predictors. All GAMs were statistically significant (F tests, $p < 0.05$ across frequency bands), confirming that the evaluated predictor sets explain a non-random fraction of the observed RNL variability. For the RF models, statistical significance in the classical sense cannot be assessed via p values. Model performance is therefore evaluated comparatively, based on explained variance (adjusted R^2).

The frequency-dependent effects and relative importance of the individual predictors inferred from the GAMs and RF models are illustrated in Fig. S5 in the supplementary material, providing insight into how the explanatory power of the multivariate models is distributed across predictors and frequency bands.

Overall model performance is summarized in Table III, which reports mean adjusted R^2 values averaged over all 37

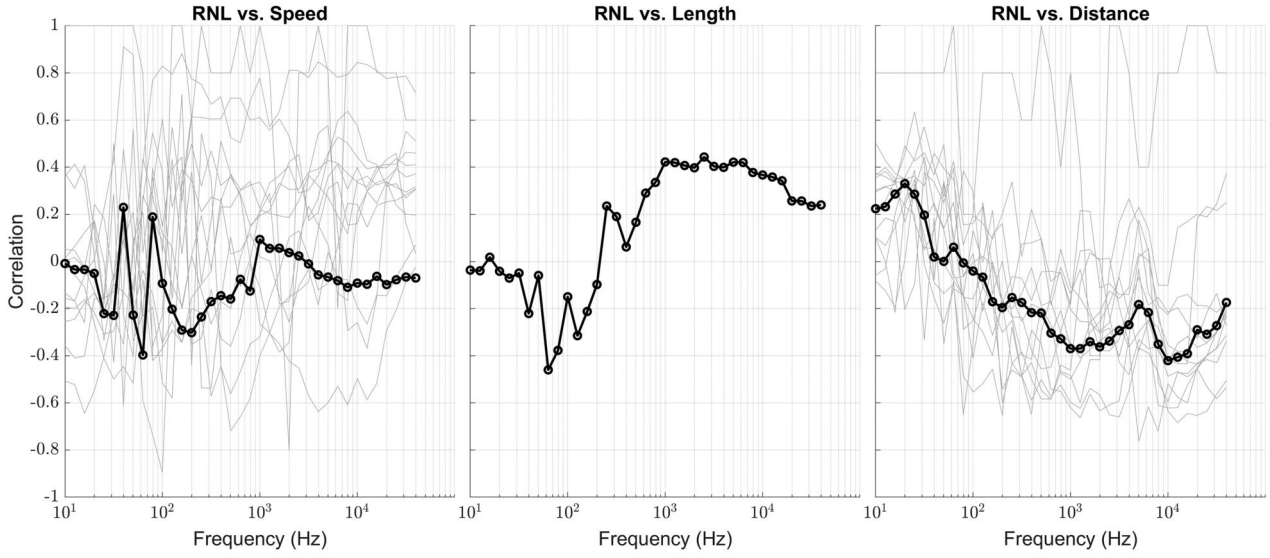

FIG. 7. Spearman correlation coefficients of the RNLs with speed, length, and distance. Gray lines represent correlations with individual vessels.

TABLE III. Mean adjusted R^2 of GAMs and RF models, averaged over all 37 frequency bands, for different combinations of parameters.

Combination of parameters	Mean adjusted R^2 for: GAMs	RF models
Speed + MMSI + distance + propulsion	0.74	0.78
Speed + length + distance + propulsion	0.72	0.75
Speed + length + distance	0.69	0.69
Speed + length + MMSI	0.62	0.61
Speed + length + propulsion	0.60	0.53
Length + distance	0.57	0.60
Speed + length	0.55	0.60
Speed + distance	0.48	0.57

frequency bands. In contrast to the bivariate analyses, the multivariate GAMs and RF models show substantially higher explanatory power. For both GAM and RF, the highest adjusted R^2 values were obtained when including MMSI as a categorical variable, reaching 0.74 for GAM and 0.78 for RF. This suggests that vessel-specific characteristics, which are not explicitly captured by the other parameters, have a substantial influence on RNLs, contributing to variability within the CTV class.

Although including MMSI yielded the best performance, it is not usable for predictive modelling beyond the observed vessels. Including ship length instead provides nearly comparable adjusted R^2 values (0.72 for GAM and 0.75 for RF) when combined with speed, distance, and propulsion type. This indicates that length may serve as a proxy for ship-specific factors such as operational state or engine configuration that are not explicitly considered in the GAMs or RF models. The consistently strong contribution of length across frequencies further supports this interpretation.

Among the individual predictors, speed and length were the most influential variables in the multivariate models, as reflected by their contribution to the adjusted R^2 values across frequency bands. This refers to their relative contribution within the GAM and RF frameworks, rather than their isolated bivariate relationships with RNL. The combination of speed, length, and distance still yielded a high explanatory power (0.72 for GAM and 0.75 for RF), reinforcing the importance of these three parameters when considered jointly. Notably, models that included only speed and length showed a noticeable drop in adjusted R^2 (0.57 for GAM, 0.60 for RF), highlighting that while these variables are important contributors, they alone do not fully explain the variations in RNL. The overall contribution of the propulsion type to the models was lower than expected. This suggests that the influence of propulsion type is secondary compared to ship length and speed or that its effects are masked by other vessel-specific parameters. GAM and RF produced comparable adjusted R^2 across most combinations of parameters, with no consistent advantage for either method. In some frequency bands and for some parameter combinations, GAMs performed slightly better, while in others, RFs provided higher explanatory power.

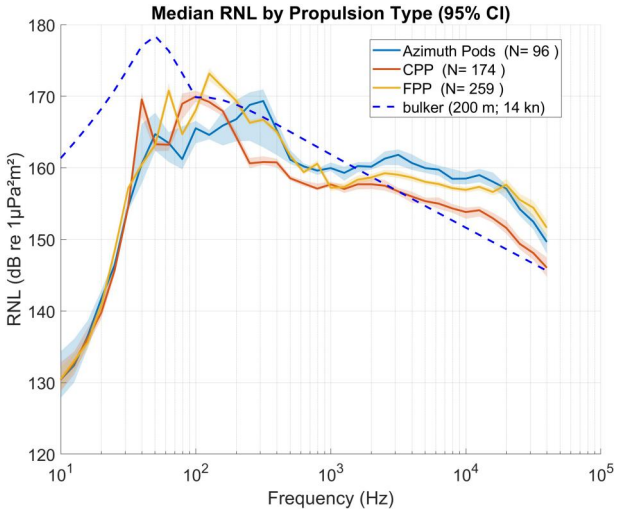

FIG. 8. Median RNLs for the different propulsion types with 95% confidence intervals.

The strong performance of models including MMSI further indicates that individual vessel characteristics, not explicitly captured by speed or length alone, play a crucial role in shaping the observed variability.

To further investigate the role of the propulsion type, we examined both the median RNLs and the proportion of passages exceeding the bulker reference spectrum per propulsion type (Figs. 8 and 9).

The characteristics of the RNL for the three propulsion types are distinct and statistically significantly different over all frequency bands above 30 Hz. Although the spectral differences are moderate in magnitude, they show that propulsion configuration can shift the CTV spectra closer to or further away from the bulker reference spectrum at specific frequencies. Notably ships with CPP more frequently remained below the bulker reference curve above 1 kHz than vessels with azimuth pods or FPPs. Interestingly, they also exhibited slightly higher average speeds (Fig. 9, right panel), further indicating that quieter performance does not necessarily result from lower operating speeds. However, the sample size (13 vessels) in this study is too low to draw general conclusions about this dependence. It is further noteworthy that CTVs with APs tend to exhibit the highest median RNLs between 1 and 20 kHz, while FPP-driven vessels show the highest RNLs above 20 kHz. The elevated levels above 20 kHz are consistent with the emission characteristics of ultrasonic antifouling devices for two FPP-equipped CTVs (CTVs 9 and 11 in Fig. S1 in the supplementary material), although this interpretation requires further verification.

IV. DISCUSSION

This study analyzed a comprehensive dataset comprising 529 CTV passages and calculated the respective RNLs of 13 individual vessels. Although vessel speed, length, and propulsion type do exert frequency-dependent effects on the RNLs, the dominant source of variability lies in vessel-specific

https://doi.org/10.1121/10.0043324

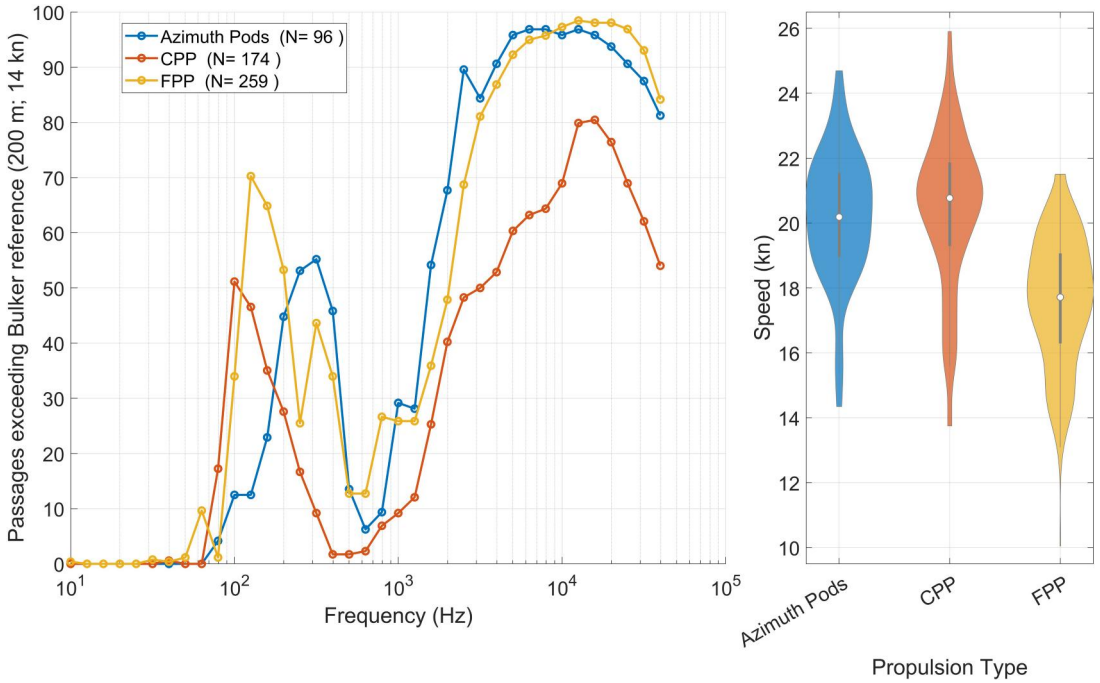

FIG. 9. Fraction of CTV passages that exceed the bulker reference RNL spectrum (200 m, 14 kn) per propulsion type (left) and violin plots of speeds per passage per propulsion type (right). Violin plots were created using the VIOLINPLOT-MATLAB toolbox by Bechtold (2016).

characteristics that are not captured by any single parameter. As such, the speed–length scaling proposed by the J-E model (MacGillivray and de Jong, 2021) does not adequately explain the observed variability in CTV SLs. However, the observed variability in RNLs was relatively low, which suggests that the measured spectrum can serve as viable input for numerical models aiming to include transiting CTVs—a vessel class that has not yet been considered in previous modeling efforts.

This study followed recommendations of the ISO 17208-3 standard for measuring underwater noise levels from vessels in shallow water (ISO, 2025). SSCI-based propagation loss corrections, including frequency-dependent absorption, were applied. Despite this, a residual distance dependence at high frequencies remains evident in the data (Fig. 7). Varying the sediment type within the SSCI framework did not remove this dependence, indicating that sediment choice alone is unlikely to be the dominant cause. We therefore interpret the remaining distance dependence as a small residual underestimation of propagation loss at higher frequencies. Such an underestimation could arise from additional loss mechanisms that are not explicitly accounted for in the applied propagation-loss models: for example, losses at the sea surface due to wave roughness or near-surface bubble layers.

Although the reported SL measurements are limited to 13 different vessels, the low variability over the 529 recorded passages suggests that the mean result can serve as a useful estimation for the SL spectrum of transiting CTVs. The observed speed distributions were concentrated in the transiting regime (Table II; see Fig. 9, right panel), and our analysis cannot resolve how SLs scale outside transit. Given that vessel-specific variability proved to be the main source of RNL variation, expanding the dataset to include more individual CTVs would be necessary to establish a more robust and generalizable source model for this vessel type. Moreover, RNLs are expected to vary significantly across different operational states. Dedicated measurements of maneuvering CTVs—particularly while pushing against wind turbine foundation for crew transfer—would be necessary to complement the findings of this study.

The inclusion of frequencies up to 40 kHz, although beyond the formal applicability range of ISO 17208-3, proved informative by revealing distinct high-frequency emissions in a subset of vessels, which would not have been detected in a strictly band-limited analysis and warrant further dedicated investigation.

When comparing our measurements to the bulker reference RNL curve (200 m, 14 kn), we find that CTVs emit comparable or higher RNLs over large parts of the spectrum, particularly between 100 and 500 Hz and above 1 kHz (Figs. 4, 5, 8, and 9).

This aligns with findings from Hermannsen *et al.* (2025), who observed elevated high-frequency noise emissions from fast vessels, and with Shipton *et al.* (2025), who showed that small vessels can emit noise levels comparable to or even exceeding those of larger commercial ships. Because the bulker reference curve is not a regulatory threshold, our comparison is not intended as a compliance assessment. Instead, it provides a contextual benchmark that situates CTV noise emissions relative to those of larger commercial vessels. The results show that CTVs can emit RNLs comparable to those of much larger ships, particularly above 1 kHz, underscoring their relevance for regional noise modelling and impact assessment.

Although this study provides valuable insight into transiting noise emissions from CTVs, future work should focus on expanding the dataset to include a wider range of individual vessels and, importantly, other operational states. Measuring CTVs during operations within offshore wind farms—particularly during crew transfers—will be crucial for a complete assessment of their underwater noise impact.

V. CONCLUSION

This study presents the first dedicated measurements of RNLs from CTVs and demonstrates that transiting CTVs, although relatively small, emit noise levels comparable to those of much larger commercial vessels, reaching or exceeding a representative large-vessel reference spectrum in several frequency bands, particularly above 1 kHz. The generally low variability in RNLs allows the derived spectra to be used as viable input for numerical models that aim to include transiting CTVs. Within the observed transit speed range, the main source of variability was found to be vessel-specific and not be explained by speed and length alone. Although residual distance-related effects at high frequencies remain evident in the data, the application of SSCI-based propagation loss correction including frequency-dependent absorption proved to be a robust and practical approach for the present measurement configuration. In this extended form, the ISO-17208-3 framework provides a feasible approach for opportunistic ship noise measurements—an area still lacking standardized methodology—and is compatible with ongoing national monitoring efforts.

SUPPLEMENTARY MATERIAL

See the supplementary material for Figs. S1–S5, including Fig. S1 for vessel-specific RNL spectral probability densities for all 13 CTVs, Figs. S2 and S3 for comparisons of SSCI and the image source propagation-loss model highlighting the contribution of the absorption term, Fig. S4 for additional scatterplots (speed, length, and distance vs RNL), and Fig. S5 for trend summaries of effect strengths and feature importances from the GAM and RF analyses.

ACKNOWLEDGMENTS

This research was funded under the DEMASK Project by the North Sea Region of the European Regional Development Fund (Interreg) of the European Union. We would like to thank the crews of the BSH research vessel *WEGA* and the WSV vessel *Neuwerk*, without whom data collection would have been impossible.

AUTHOR DECLARATIONS

Conflict of Interest

The authors have no conflicts to disclose.

Ethics Approval

This study did not involve human participants or live animals. Ethics approval was therefore not required.

DATA AVAILABILITY

The raw hydrophone recordings and high-resolution SPL time series used in this study are subject to third-party restrictions and cannot be made publicly available due to national data protection regulations. The authors are not permitted to distribute these data. Processed data products that support the findings of this study, including aggregated decidecade-band SPL statistics at 20 s temporal resolution and derived spectral metrics, will be deposited in the ICES Continuous Noise Database (https://underwaternoise.ices.dk/continuous).

Bechtold, B. (**2016**). "Violin plots for Matlab," GitHub, https://github.com/bastibe/Violinplot-Matlab.

Brandt, M., Diederichs, A., Betke, K., Matuschek, R., and Nehls, G. (**2011**). "Responses of harbour porpoises to pile driving at the Horns Rev II offshore wind farm in the Danish North Sea," Mar. Ecol. Prog. Ser. **421**, 205–216.

Breiman, L. (**2001**). "Random forests," Mach. Learn. **45**, 5–32.

DEMASK Project (**2025**). "The DEMASK Project, Interreg North Sea," https://www.interregnorthsea.eu/demask (Last viewed 13 April 2026).

Duarte, C. M., Chapuis, L., Collin, S. P., Costa, D. P., Devassy, R. P., Eguíluz, V. M., Erbe, C., Gordon, T. A. C., Halpern, B. S., Harding, H. R., Havlik, M.-N., Meekan, M. G., Merchant, N. D., Miksis-Olds, J., Parsons, M., Predragovic, M., Radford, A. N., Radford, C. A., Simpson, S. D., Slabbekoorn, H., Staaterman, E., van Opzeeland, I., Winderen, J., Zhang, X., and Juanes, F. (**2021**). "The soundscape of the Anthropocene ocean" Science **371**, eaba4658.

Erbe, C., Dunlop, R. A., and Dolman, S. J. (**2018**). "Effects of noise on marine mammals," in *Effects of Anthropogenic Noise on Animals*, edited by H. Slabbekorn, R. Dooling, A. Popper, and R. Fay (Springer, New York), pp. 277–309.

Hawkins, A. D., and Popper, A. N. (**2017**). "A sound approach to assessing the impact of underwater noise on marine fishes and invertebrates," ICES J. Mar. Sci. **74**(3), 635–651.

Hermannsen, L., Ladegaard, M., Tønnesen, P., Malinka, C., Beedholm, K., Tougaard, J., Rojano-Doñate, L., Tyack, P. L., and Madsen, P. T. (**2025**). "High-frequency vessel noise can mask porpoise echolocation," J. Exp. Biol. **228**(6), jeb249963.

IEC (**2014**). "IEC 61260-1:2014—Electroacoustics—Octave-band and fractional-octave-band filters—Part 1: Specifications" (International Electrotechnical Commission, Geneva, Switzerland).

IEC (**2016**). "IEC 61260-3:2016—Electroacoustics—Octave-band and fractional-octave-band filters—Part 3: Periodic tests" (International Electrotechnical Commission, Geneva, Switzerland).

IEC (**2019**). "IEC 60565-2:2019—Underwater acoustics—Hydrophones—Calibration of hydrophones—Part 2: Procedures for low frequency pressure calibration," 1st ed. (International Electrotechnical Commission, Geneva, Switzerland).

ISO (**2016**). "ISO 17208-1:2016/Amd 1:2024—Underwater acoustics—Quantities and procedures for description and measurement of underwater sound from ships—Part 1: Requirements for precision measurements in deep water used for comparison purposes [includes Amendment 1: 2024]" (International Organization for Standardization, Geneva, Switzerland).

ISO (**2019**). "ISO 17208-2:2019—Underwater acoustics—Quantities and procedures for description and measurement of underwater sound from ships—Part 2: Determination of source levels from deep water measurements" (International Organization for Standardization, Geneva, Switzerland).

ISO (**2025**). "ISO 17208-3:2025—Underwater acoustics—Quantities and procedures for description and measurement of underwater sound from ships—Part 3: Requirements for measurements in shallow water" (International Organization for Standardization, Geneva, Switzerland).

JOMOPANS Project (**2020**). "Joint Monitoring Programme for Ambient Noise in the North Sea (JOMOPANS), Interreg North Sea," https://northsearegion.eu/jomopans/ (Last viewed 13 April 2026).

Juretzek, C., Schmidt, B., and Boethling, M. (**2021**). "Turning scientific knowledge into regulation: Effective measures for noise mitigation of pile driving," J. Mar. Sci. Eng. **9**(8), 819.

Macaulay, J. D. J., Malinka, C. E., Gillespie, D., and Madsen, P. T. (**2020**). "High resolution three-dimensional beam radiation pattern of harbour porpoise clicks with implications for passive acoustic monitoring," J. Acoust. Soc. Am. **147**(6), 4175–4188.

MacGillivray, A. O., and de Jong, C. A. F. (**2021**). "A reference spectrum model for estimating source levels of marine shipping based on automated identification system data," J. Mar. Sci. Eng. **9**(4), 369.

Malinka, C., Atkins, J., Johnson, M., Tønnesen, P., Dunn, C., Claridge, D., Aguilar de Soto, N., and Madsen, P. (**2020**). "An autonomous hydrophone array to study the acoustic ecology of deep-water toothed whales," Deep Sea Res., Part A **158**, 103233.

McMorland, J., Flannigan, C., Carroll, J., Collu, M., McMillan, D., Leithead, B., and Coraddu, A. (**2022**). "A review of operations and maintenance modelling with considerations for novel wind turbine concepts," Renewable Sustainable Energy Rev. **165**, 112581.

Merchant, N. D., Barton, T. R., Thompson, P. M., Pirotta, E., Dakin, D. T., and Dorocicz, J. (**2013**). "Spectral probability density as a tool for ambient noise analysis," J. Acoust. Soc. Am. **133**(4), EL262–EL267.

Shipton, M., Obradović, J., Mišković, N., and Diamant, R. (**2025**). "Underwater radiated noise characteristics of small vessels—An analysis of the HearMyShip database," Mar. Pollut. Bull. **216**, 117903.

SOUND Mapping Project (**2021**). *SOUND mapping—Akustische Kartierung in der Deutschen AWZ von Nord- und Ostsee* (*SOUND mapping—Acoustic mapping in the German Exclusive Economic Zone of the North and Baltic Seas*), https://www.bsh.de/DE/THEMEN/Forschung_und_Entwicklung/Abgeschlossene-Projekte/SOUND-Mapping/sound-mapping_node.html (Last viewed 13 April 2026).

Urick, R. J. (**1983**). *Principles of Underwater Sound*, 3rd ed. (McGraw-Hill, New York), pp. 131–132.

Ward, J., Wang, L., Robinson, S., and Harris, P. (**2021**). "Standard for data processing of measured data," Report of the EU Interreg Joint Monitoring Programme for Ambient Noise North Sea (JOMOPANS), National Physical Laboratory (NPL), Teddington, UK, pp. 5–7.

Wood, S. (**2017**). *Generalized Additive Models: An Introduction with R*, 2nd ed. (Chapman and Hall, New York).

Yubero, R., de Jong, C. A. F., Ainslie, M. A., MacGillivray, A. O., and Wang, L. (**2025**). "Measuring vessel source level in shallow water using the smoothed semi-coherent image method," J. Acoust. Soc. Am. **157**(3), 1938–1954.